10th World Congress on Structural and Multidisciplinary Optimization
May 19 - 24, 2013, Orlando, Florida, USA

Topology optimization of dielectric ring resonators in application on laser resonators and optical sensors

Akihiro Takezawa[1], Masanobu Haraguchi[2], Toshihiro Okamoto[3], Mitsuru Kitamura[4]

[1]Department of Mechanical System and Applied Mechanics, Graduate School of Engineering, Hiroshima University, 1-4-1 Kagamiyama, Higashi-Hiroshima, Hiroshima, Japan, akihiro@hiroshima-u.ac.jp
[2]Department of Optical Science and Technology, Faculty of Engineering, The University of Tokushima, 2-1 Minamijousanjima, Tokushima, Tokushima, Japan, haraguti@opt.tokushima-u.ac.jp
[3]Department of Optical Science and Technology, Faculty of Engineering, The University of Tokushima, 2-1 Minamijousanjima, Tokushima, Tokushima, Japan, okamoto@opt.tokushima-u.ac.jp
[4]Department of Mechanical System and Applied Mechanics, Graduate School of Engineering, Hiroshima University, 1-4-1 Kagamiyama, Higashi-Hiroshima, Hiroshima, Japan, kitamura@hiroshima-u.ac.jp

1. Abstract
Optimal cross-sectional shapes of whispering-gallery ring resonators with prescribed emission wavelength and resonance mode are generated using topology optimization based on the finite element method considering the application of the laser resonators and optical biosensors. In the laser resonator optimization, the two critical performance indices, the quality factor (Q factor) and mode volume of a resonator, are treated as the objective functions in the optimization. In the optical biosensor optimization, the Q factor and energy density of the specified domain are treated as the objective functions. The sensitivity of the objective function is derived based on the adjoint variable method. Based on these formulations, an optimization algorithm is constructed using the method of moving asymptotes (MMA) . We provide numerical examples to illustrate the validity and utility of the proposed methodology.
2. Keywords: Topology optimization, optical resonators, whispering gallery modes, modal sensitivity analysis

3. Introduction

Micro-ring resonators have tremendous potential in optics with applications to low threshold microcavity lasers and optical sensors. [1, 2]. The optical modes, set up in these devices by emissions from input light, form circular continuous closed beams governed by internal reflections along the boundary of the resonator. The circular mode shape is called a whispering-gallery mode (WGM). Optical resonators exploiting WG modes have been attaining high levels in the important typical-performance criteria for resonators, *i.e.*, high quality factor (Q factor) which measures the inverse of the decay rate of the energy and low mode volume which signifies the spatial confinement of the light [3]. In other words, the light wave is trapped within a very small volume during WG mode emission. Since the behavior of the trapped light is very sensitive to changes in the device's shape or surroundings, the use of the WGM resonator as a sensor was studied. The representative example used here is label-free bio-sensing. The optical path in the WGM device can be changed even by the binding of molecules. The variation in the optical path can be detected as a shift in the resonance wavelength [4, 2].

In this research, the optimization methodology to enhance the performance of the WGM resonator is studied in the application of the laser resonators and optical biosensors. Topology optimization [5] has contributed to optimal designs in novel wave propagation devices in photonics [6, 7, 8, 9]. In the approach, the designed devices are represented as distributions of the dielectric material or metal in the analysis model. By updating the distribution by the gradient-based optimization method, the generated distribution represents the shape of devices that attain specific performance criteria.

In this research, we study and identify optimal shapes for WG micro-ring resonators using FEM-based topology optimization. The systematic procedure helps to find optimal device shapes with fixed design performance given a prescribed emission wavelength and WG resonance mode. The analysis domains and the equations of state for the WG mode ring resonators are first considered. In the laser resonator optimization, the two critical performance indices, the quality factor (Q factor) and mode volume of a resonator, are treated as the objective functions in the optimization. In the optical biosensor optimization, the Q factor and energy density of the specified domain are treated as the objective functions. The emission wavelength is formulated as an equality constraint. The methodology is implemented as a

distribution optimization of the dielectric material using the solid isotropic material with the penalization (SIMP) method of topology optimization. The optimization algorithm is constructed based on the two-times FEM analysis, sensitivity analysis for each objective function and density function constraint, and sequential linear programming (SLP) with a phase field method [10]. Finally, numerical examples are provided as a validation of the proposed methodology.

4. Problem settings

4.1 Analysis model

Using cylindrical coordinates, we model a WG ring resonator centered on the origin in free space as illustrated in Fig. 1. The coordinate system composed of components (z, ϕ, r) are the axial, azimuthal, and radial coordinates respectively. The vertical cross-sectional shape of the device in the z-r plane, is treated as the design target; we obtain the final axisymmetric form by generating the solid of revolution. The domain is enclosed by a perfect matched layer (PML) domain.

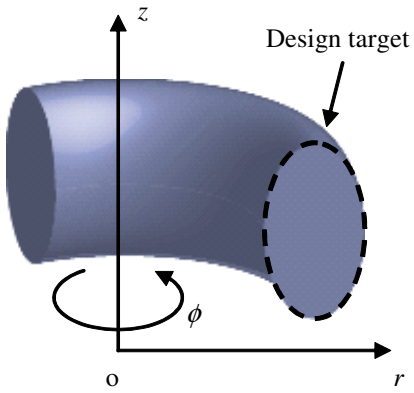

Figure 1: The analysis and design domain as described by cylindrical coordinates

4.2 Equations of state

The equations of state representing resonance-mode wave propagation within the domain are the 3D vector Helmholtz equations. If the resonator medium is isotropic, the Helmholtz equation for the magnetic field $\boldsymbol{H}$, as derived from Maxwell's equation, is written as follows:

$$\nabla \times \left(\frac{1}{\epsilon} \nabla \times \boldsymbol{H} \right) - \frac{1}{c^2} \frac{\partial^2 \boldsymbol{H}}{\partial t^2} = 0 \tag{1}$$

where ϵ is the relative permittivity and c the speed of light. Here, the time harmonic function is assumed in the form $\boldsymbol{H}(\boldsymbol{x}, t) = \boldsymbol{H}(\boldsymbol{x}) e^{i\omega t}$ and the above equation is solved as an eigenvalue problem by FEM, where $\omega = 2\pi f$ is the angular resonance frequency given resonance frequency f. To suppress spurious modes in the analysis, a weak penalty term [11] is introduced to yield the following modified equation used in [12]:

$$\nabla \times \left(\frac{1}{\epsilon} \nabla \times \boldsymbol{H} \right) - \alpha \nabla \left(\nabla \cdot \boldsymbol{H} \right) + \frac{\omega^2}{c^2} \boldsymbol{H} = 0 \tag{2}$$

where α is a coefficient. The following two types of boundary conditions for the above equation are considered:

$$\boldsymbol{H} \times \hat{\boldsymbol{n}} = 0 \text{ on } \Gamma_{\text{pmc}} \tag{3}$$

$$\hat{\boldsymbol{n}} \times \nabla \times \boldsymbol{H} + ik \hat{\boldsymbol{n}} \times \hat{\boldsymbol{n}} \times \boldsymbol{H} = 0 \text{ on } \Gamma_{\text{abc}} \tag{4}$$

where k is the wave number in free-space and $\hat{\boldsymbol{n}}$ is the unit vector normal to the boundary; the former describing perfect magnetic conduction and the latter first-order absorption on the boundary.

The state variable is the set comprising the time-dependent radial, azimuthal, and axial components of the magnetic field vector $\boldsymbol{H}(\boldsymbol{r}, t)$. We factorize the azimuthal-dependence from the variable using the cylindrical coordinate system; that is,

$$\boldsymbol{H}(\boldsymbol{r}) = e^{iM\phi} [H_r(r, z), iH_\phi(r, z), H_z(r, z)]^T \tag{5}$$

where M is the azimuthal mode order.

4.3 Performance criteria

In our analysis, the performance criteria in designing WGM laser resonator are the Q factor and the mode volume. In calculating the Q factor, we consider only the radiation loss for which, Q_{rad} is calculated as follows [3, 13]:

$$Q_{\mathrm{rad}} = \frac{\mathrm{Re}(f)}{2\mathrm{Im}(f)} \tag{6}$$

where $\mathrm{Re}(\cdot)$ and $\mathrm{Im}(\cdot)$ represent respectively the real and imaginary parts of the variable. In the analysis for the domain surrounded by the PLM domain, the real part of the frequency represents the total energy of the domain, whereas the imaginary part represents the rate of energy absorption by the PLM domain, *i.e.* the radiation loss (Chapter 5 in [14]).

In addition, the mode volume is formulated as follows [3, 13]:

$$V_{\mathrm{mode}} = \frac{\int_\Omega \epsilon |\boldsymbol{E}|^2 dx}{\max(\epsilon |\boldsymbol{E}|^2)} \tag{7}$$

where Ω denotes the analysis domain and $\boldsymbol{E}$ is the electric field vector.

In addition to the Q factor, the performance criteria for the sensor design are the energy density of the detection domain formulated as follows:

$$U = \frac{\int_{\Omega_{\mathrm{det}}} \epsilon |\boldsymbol{E}|^2 dx}{\int_{\Omega_{\mathrm{det}}} dx} \tag{8}$$

4.4 Topology optimization

Topology optimization is performed based on density or SIMP interpolation schemes; here SIMP stands for solid isotropic material with penalization [5]. The relative permittivity over the design domain is expressed in terms of a density function ρ, $(0 \leq \rho \leq 1)$:

$$\epsilon = \epsilon_{\mathrm{Air}} + \rho(\epsilon_{\mathrm{GaAlAs}} - \epsilon_{\mathrm{Air}}). \tag{9}$$

The optimal cross-sectional shape of the device can then be specified as a distribution in ρ.

During optimization, we target the following three tasks in the laser resonator optimization:

1. Maximization of the Q factor associated with emissions as expressed by equation 8.
2. Minimization of the mode volume as expressed by equation 7.
3. Specification of the emission wavelength $\lambda = c/\mathrm{Re}(f)$,.

Task 3) is first assumed to be satisfied by introducing the corresponding equality constraint. In the eigenfrequency analysis, assuming normalized eigenmodes $\boldsymbol{H}$ ($\int_\Omega |\boldsymbol{H}|^2 dx = 1$), the total electric energy over the analysis domain equals the square of the angular eigenfrequency ($\int_\Omega \epsilon |\boldsymbol{E}|^2 dx = \mathrm{Re}(\omega)^2$) [15, 16]. That is, by pre-specifying emission wavelength and azimuthal mode order, both numerators in the expressions for the Q-factor and mode volume are constant during optimization. Thus, the objective functions for Task 1, J_Q, and Task 2, J_V, and the equality constraint h for Task 3 are formulated as follows:

$$\underset{\rho}{\mathrm{minimize}}\, J_Q(\rho) = \mathrm{Im}(f) \tag{10}$$

or

$$\underset{\rho}{\mathrm{minimize}}\, J_V(\rho) = -\max(\epsilon |\boldsymbol{E}|^2) \tag{11}$$

subject to

$$h(\rho) = \lambda - \lambda_0 = 0 \tag{12}$$

with λ_0 denoting the specified wavelength.

In the sensor optimization, we target the following three tasks in the laser resonator optimization:

1. Maximization of the energy density of the specified domain.
2. Maximization of the Q factor associated with the emissions as expressed by 8.
3. Specification of the emission wavelength $\lambda = c/\mathrm{Re}(f)$.

Handling the Q factor as the same way with the laser resonator optimization, the following objective functions are formulated:

$$\underset{\rho}{\text{minimize}}\, J_U(\rho) = -\int_{\Omega_{\text{det}}+\Omega_{\text{ec}}} \epsilon |\boldsymbol{E}|^2 dx \tag{13}$$

or

$$\underset{\rho}{\text{minimize}}\, J_Q(\rho) = \mathrm{Im}(f) \tag{14}$$

subject to

$$h(\rho) = \lambda - \lambda_0 = 0 \tag{15}$$

4.5 Numerical implementation and optimization algorithm
We solve the eigenvalue problem in equation 2 by FEM. To perform the iterating numerical optimization based on the FEM result, the target WG eigenmode is required to be automatically selected from the numerous resulting eigenmodes. The two-step analysis proposed in [12] is introduced to specify the target mode during the optimization iteration. First, we solve the small closed finite-element model composed of the device surrounded by a perfect magnetic wall to obtain the eigenfrequency of the target WG mode. The first eigenmode of the model corresponds to the target WG mode. Second, we solve for the original model surrounded by PLM domains, as drawn in Fig. 2, specifying the target eigenfrequency obtained by the closed model.

Since the density function is updated by gradient-based algorithms, sensitivities for both objective function and constraint must be calculated. The sensitivity of the objective function in equation (13) and the equality constraint in equation (15) can be calculated from only state variables without solving the adjoint equation because the optimization problem of the eigenfrequency is self-adjoint [17]. The sensitivity of the objective function in equation (14) is expressible in terms of the functions of the state variable and its adjoint; the adjoint equation is as formulated in [18].

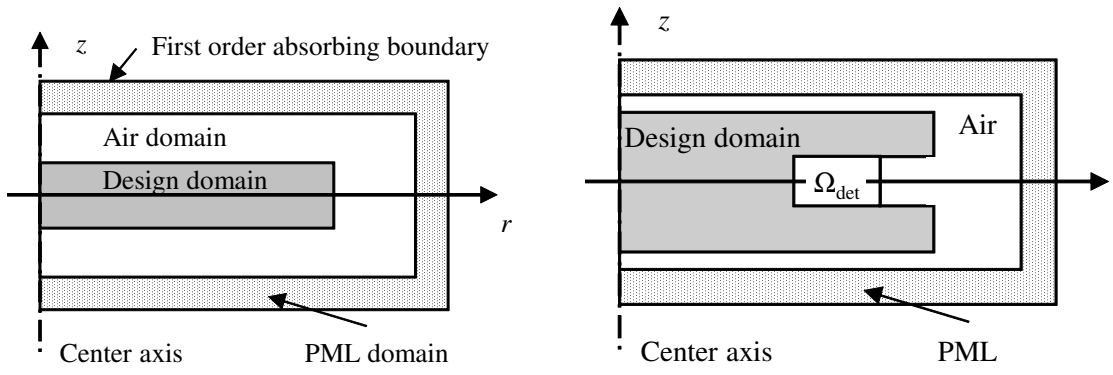

(a) (b)

Figure 2: The analysis domains used in FEM for (a) laser optimization and (b) sensor optimization.

5. Numerical examples
To confirm the validity of the proposed methodology, some numerical examples are studied. The detail

of the computational model is first explained. Optimizations are performed with specified TE modes ($p = 1,\ M = 10 or 11$). The size of each is as follows: the air domains of both closed and open models are 1.8 μm $\times$ 3 μm and 4 μm $\times$ 6 μm respectively; the design domain which is identical in both models is 1.5 μm $\times$ 2 μm. The PLM domains are set for the upper, lower and right-side of the open model and their thickness are all 0.25 μm. The design domain is meshed by 75 $\times$ 100 square elements. The other domains are meshed by triangular elements. The design variable is discretized as a piecewise-constant function on the square finite elements of the design domain. Assuming horizontal mirror symmetry of the optimal shapes, only the upper half of the design domain is optimized. Thus, the 7500 design variables are updated during optimization in this problem. The media constituting the resonator and surrounding domain are assumed to be respectively isotropic GaAlAs with $\epsilon = 11.2896$ and air with $\epsilon = 1$. All FEMs are performed using a commercial software, COMSOL Multiphysics.

5.1 Optimization of laser resonator

The first optimization is performed with the specified wavelength $\lambda_0 = 1200$nm and azimuthal mode order $M = 11$ targeting to improve the Q factor using the objective function in equation 13. Fig. 3 shows the optimal configuration, the distribution of the electric energy density $\epsilon|E|^2$ and the electric field intensity $|E|^2$. These figures are shown in 1.5 μm $\times$ 2 μm boxes for which the left side corresponds to the center axis. The resulting Q factor and mode volume are $Q_{\mathrm{rad}} = 5.809 \times 10^7,\ V_{\mathrm{mode}} = 1.716 \times 10^{-19}$. The optimal shape has a large smooth convex form covering the electric-field hot spot to reduce radiation losses.

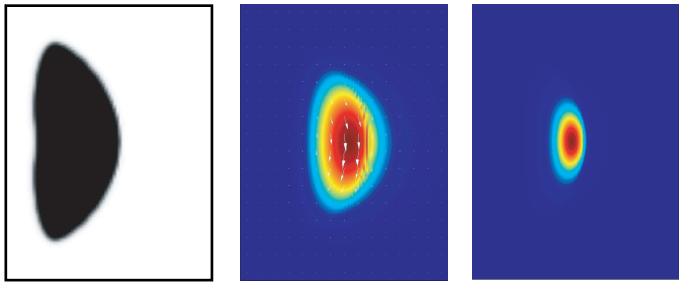

(a) (b) (c)

Figure 3: Optimal result obtained by maximization of Q_{rad} with $\lambda_0 = 1200$nm and $M = 11$. (a) Optimal shape. (b) Electric field intensity $|E|^2$ distribution, with the white arrows indicating the electric field's magnitude and direction in the medial plane. (c) Electric energy density $\epsilon|E|^2$ distribution.

The optimizations are performed with the view to increasing Q factor and decreasing mode volume as far as possible. The following objective function is introduced by integrating equations 13 and 14 using weighting factor w:

$$\underset{\rho}{\text{minimize}}\, J(\rho) = w * \mathrm{Im}(f) - (1 - w) * \max(\epsilon|\boldsymbol{E}|^2) \tag{16}$$

Varying the weighting coefficient from 0 to 1, six optimal results are encountered; see Fig. 4. Result (a) corresponds to that shown in Fig. 3. As a trade-off exists between Q-factor and mode volume, the set of optimal solutions forms a Pareto-optimal set [19]; better Q_{rad} values must lead to worse V_{mode} and vice versa given the same wavelength and the azimuthal mode order. Fig. 5 shows the electric field intensity corresponding to shape (f). In contrast to high Q factor shape, the low-mode-volume optimal shape has a small concave form near the center to enhance the maximum electric energy. The interpolated shapes (b)-(e) have both characteristics. The concentrations of the electric field and the electric energy at the center of the device are observed in shape (f) whereas shape (a) has a wider hot spot. Moreover, to maintain the emission wavelength for the same azimuthal mode order but different shapes, the location of the cross-section moves off-center as the cross-sectional area becomes smaller. With normalization of the eigenmode, the square of the emission frequency equals the total electric energy of the resonator and fixed. Thus, the total energy of the cross-section, which relates the area and the diameter at the center of the cross-section, are inversely related.

5.2 Optimization of optical sensor

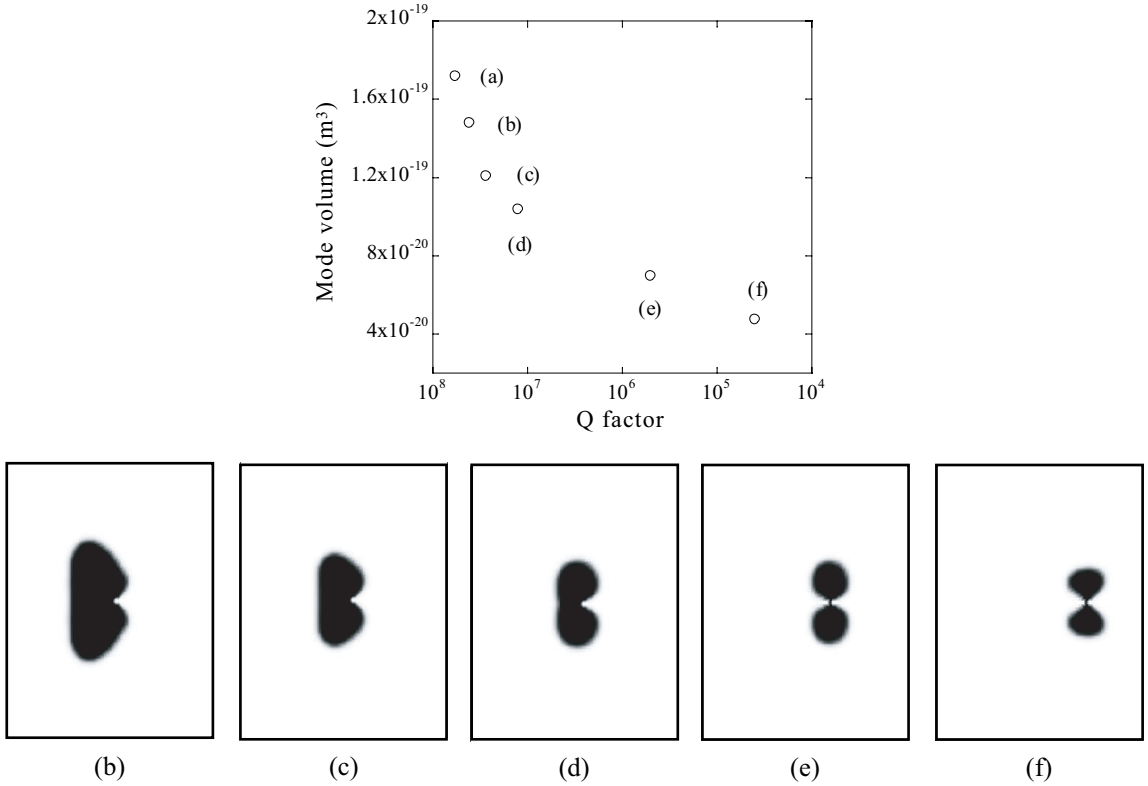

Figure 4: Optimal shapes and their performances, obtained by maximizing Q_{rad} and minimizing V_{mode} with different weighting factor settings in equation (16).

The first optimization of the optical sensor is performed to improve the energy density at the specified detection domain by using the objective function in 13. Optimizations are performed with a specified wavelength $\lambda_0 = 1300$nm. Fig. 6 shows the optimal configuration obtained at iteration 39, the distribution of the electric energy density $\epsilon|E|^2$ and the electric field intensity $|E|^2$. These figures are shown in 1.5 μm $\times$ 2 μm boxes, where the left side corresponds to the center axis. The small squares shown in Fig. 6(a) and (b) represent the detection domain Ω_{det} and the energy concentration domain Ω_{ec}. Both domains are shown side by side in each figure; however, one of them is less visible because of the surrounding colors in Fig. 6(a) and (b). The resulting energy density and Q factor are $U = 6.50 \times 10^{14}$ and $Q_{\mathrm{rad}} = 1.04 \times 10^5$, respectively. The optimal shape is concave near the energy concentration domain to enhance the maximum electric energy. As a result, a strong electric field can be observed in the detection domain. This shape is very similar to the optimal shape for minimization of the mode volume shown in the previous example.

Finally, the optimization is performed with a view to increasing both the energy density and the Q factor as far as possible. The following objective function is introduced by integrating (13) and (14) using the weighting factor w ($0 \leq w$ $le1$):

$$\underset{\rho}{\text{minimize}}\, J(\rho) = -w * \int_{\Omega_{\mathrm{det}}+\Omega_{\mathrm{ec}}} \epsilon|\boldsymbol{E}|^2 dx + (1-w) * \mathrm{Im}(f) \tag{17}$$

The location and size of the detection domain are the same as those in the first optimization example. By varying the weighting coefficient from 0 to 1, five optimal results are found; see Fig. 7. Result (a) corresponds to that shown in Fig. 6. A trade-off relationship between the Q-factor and the mode volume can be seen from these results, i.e., that better energy density must lead to a worse Q factor and vice versa, given the same wavelength and azimuthal mode order. The characteristics of these shapes can be found by analysis of the energy distribution. In Fig. 7 (b), a similar energy distribution to that of result (a) can be obtained, because the Q factor term in the objective function was weaker. In Fig. 7 (c), although the energy hot spot is next to the detection domain, relatively high energy concentrations can be observed in both the upper and lower sides of the cross-section. In Fig. 7 (d) and (e), the hot

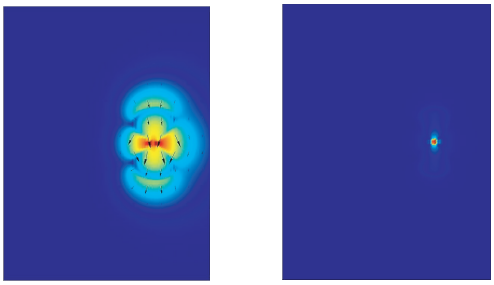

(a) (b)

Figure 5: (a) Electric field intensity $|E|^2$ distribution with black arrows indicating the electric field's magnitude and direction in the medial plane and (b) Electric energy density $\epsilon|E|^2$ distribution of optimal result shown in Fig. 4(f)

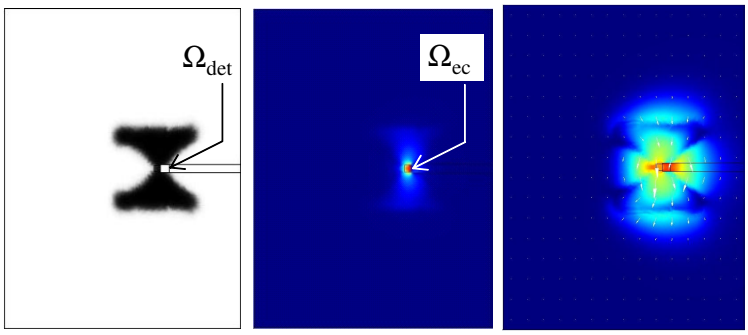

(a) (b) (c)

Figure 6: (a) Optimal shape. (b) Electric energy density $\epsilon|E|^2$ distribution. (c) Logarithmic electric field intensity $|E|^2$ distribution, where the white arrows indicate the electric field magnitude and direction in the medial plane.

spot moved away from the detection domain to reduce the energy losses. The dielectric is connected between the hot spot and the detection domain to transfer the electric energy. These results show that optimization for both high energy density and a high Q factor could be performed using the proposed methodology.

6. Conclusion

In this research, we optimized cross-sectional shapes for WGM resonators for the application of laser resonators and optical sensors using topology optimization. The systematic procedure helps to find optimal device shapes with certain designed performance given prescribed emission wavelength and WG resonance mode. As a basic principle for designing WGM laser resonators, we found that large convex shapes produced high Q factors; small concave shapes produced low mode volumes. We also found that concave shapes produced high energy density levels near the cross-sectional center of the devices in the design of optical sensors. The multi-objective optimizations were succeeded in both optimizations. Through these studies, we confirmed the utility of the topology optimization in the design of WGM devices.

7. References

[1] Kerry J. Vahala. Optical microcavities. *Nature*, 424:839–846, 2003.

[2] Frank Vollmer and Stephen Arnold. Whispering-gallery-mode biosensing: label-free detection down to single molecules. *Nature methods*, 5(7):591–596, 2008.

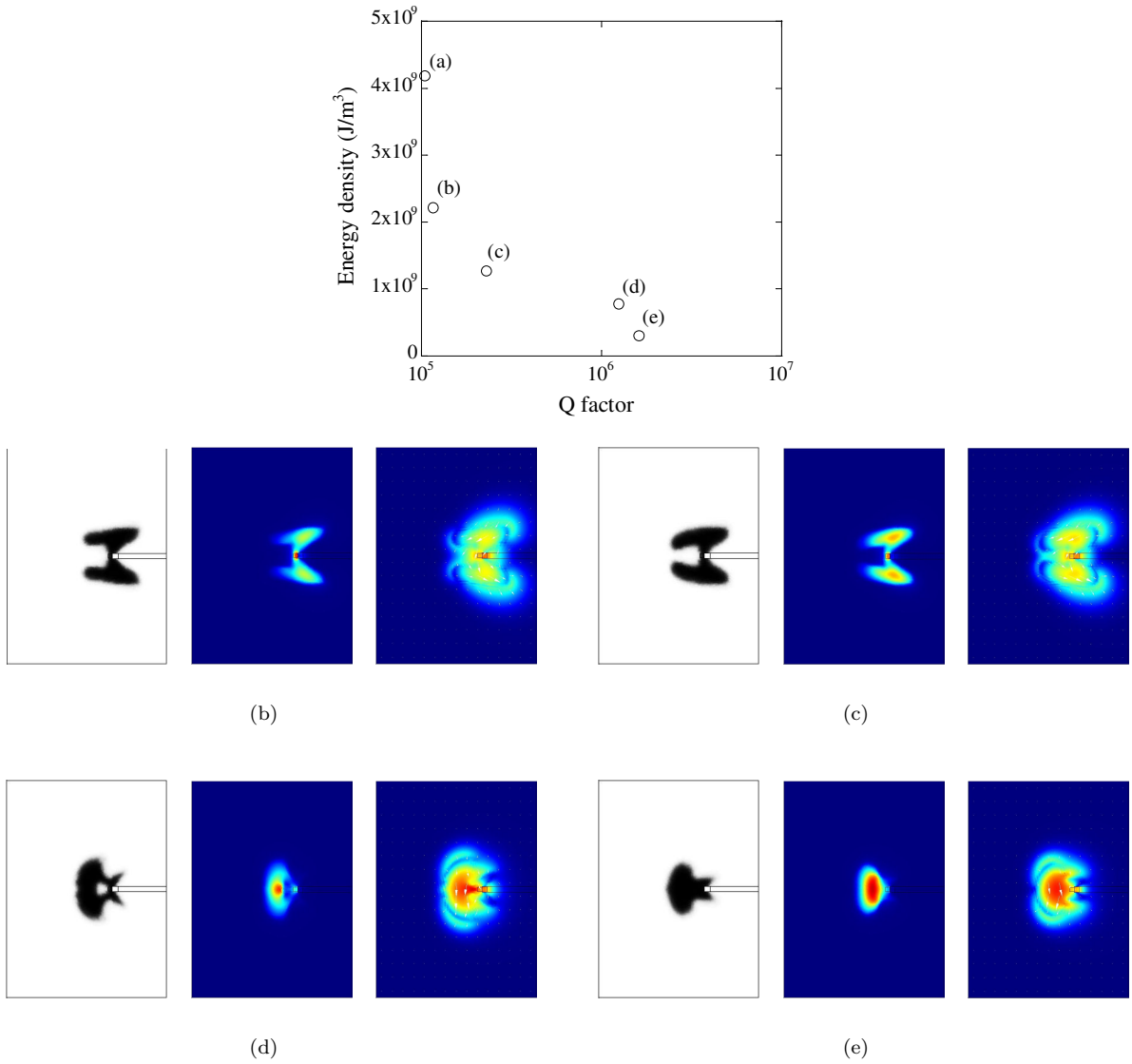

Figure 7: Optimal results obtained by maximizing the energy density and the Q factor with different weighting factor settings in (17). The left, center and right figures show the optimal configuration, energy distribution and logarithmic electric field intensity distribution corresponding to each setting.

[3] A.N. Oraevsky. Whispering-gallery waves. *Quant. Electron.*, 32(5):377–400, 2002.

[4] F. Vollmer, D. Braun, A. Libchaber, M. Khoshsima, I. Teraoka, and S. Arnold. Protein detection by optical shift of a resonant microcavity. *Appl. Phys. Lett.*, 80(21):4057–4059, 2002.

[5] M. P. Bendsøe and O. Sigmund. *Topology Optimization: Theory, Methods, and Applications.* Springer-Verlag, Berlin, 2003.

[6] J.S. Jensen and O. Sigmund. Systematic design of photonic crystal structures using topology optimization: Low-loss waveguide bends. *Appl. Phys. Lett.*, 84(12):2022–2024, 2004.

[7] W. R. Frei, D. A. Tortorelli, and H. T. Johnson. Topology optimization of a photonic crystal waveguide termination to maximize directional emission. *Appl. Phys. Lett.*, 86:111114, 2005.

[8] A. R. Diaz and O. Sigmund. A topology optimization method for design of negative permeability metamaterials. *Struct. Multidisc. Optim.*, 41(2):163–177, 2010.

[9] J. Andkjær and O. Sigmund. Topology optimized low-contrast all-dielectric optical cloak. *Appl. Phys. Lett.*, 98(2):021112, 2011.

[10] A. Takezawa, S. Nishiwaki, and M. Kitamura. Shape and topology optimization based on the phasefield method and sensitivity analysis. *J. Comput. Phys.*, 229(7):2697–2718, 2010.

[11] M. Koshiba, K. Hayata, and M. Suzuki. Improved finite-element formulation in terms of the magnetic field vector for dielectric waveguides. *IEEE Trans. Microw. Theor. Tech.*, 33(3):227–233, 1985.

[12] M. Oxborrow. Traceable 2-d finite-element simulation of the whispering-gallery modes of axisymmetric electromagnetic resonators. *IEEE Trans. Microw. Theor. Tech.*, 55(6):1209–1218, 2007.

[13] K. Srinivasan, M. Borselli, O. Painter, A. Stintz, and S. Krishna. Cavity q, mode volume, and lasing threshold in small diameter algaas microdisks with embedded quantum dots. *Optic. Express*, 14(3):1094–1105, 2006.

[14] D. W. Prather, S. Shi, A. Sharkawy, J. Murakowski, and G. J. Schneider. *Photonic Crystals, Theory, Applications and Fabrication.* Wiley, Hoboken, 2009.

[15] S. H. Gould. *Variational Methods for Eigenvalue Problems: An Introduction to the Methods of Rayleigh, Ritz, Weinstein, and Aronszajn.* Dover Publications, New York, 1995.

[16] G. Allaire. *Numerical Analysis and Optimization: An Introduction to Mathematical Modelling and Numerical Simulation.* Oxford University Press, 2007.

[17] E. J. Haug, K. K. Choi, and V. Komkov. *Design Sensitivity Analysis of Structural Systems.* Academic Press, Orlando, 1986.

[18] G. Allaire. *Conception Optimale De Structures.* Springer-Verlag, Berlin, 2007.

[19] K. Deb. *Multi-Objective Optimization Using Evolutionary Algorithms.* Wiley, Chichester, 2009.